

A new hybrid integral representation for frequency domain scattering in layered media

Jun Lai*, Leslie Greengard† and Michael O’Neil‡

July 23, 2015

Abstract

A variety of problems in acoustic and electromagnetic scattering require the evaluation of impedance or layered media Green’s functions. Given a point source located in an unbounded half-space or an infinitely extended layer, Sommerfeld and others showed that Fourier analysis combined with contour integration provides a systematic and broadly effective approach, leading to what is generally referred to as the Sommerfeld integral representation. When either the source or target is at some distance from an infinite boundary, the number of degrees of freedom needed to resolve the scattering response is very modest. When both are near an interface, however, the Sommerfeld integral involves a very large range of integration and its direct application becomes unwieldy. Historically, three schemes have been employed to overcome this difficulty: the method of images, contour deformation, and asymptotic methods of various kinds. None of these methods make use of classical layer potentials in physical space, despite their advantages in terms of adaptive resolution and high-order accuracy. The reason for this is simple: layer potentials are impractical in layered media or half-space geometries since they require the discretization of an infinite boundary. In this paper, we propose a hybrid method which combines layer potentials (physical-space) on a finite portion of the interface together with a Sommerfeld-type (Fourier) correction. We prove that our method is efficient and rapidly convergent for arbitrarily located sources and targets, and show that the scheme is particularly effective when solving scattering problems for objects which are close to the half-space boundary or even embedded across a layered media interface.

1 Introduction

Problems of acoustic and electromagnetic wave scattering in half-space or layered media geometries require the solution of the the governing partial differential equations subject to suitable boundary and radiation conditions. In the two-dimensional, time-harmonic setting, both reduce to the Helmholtz equation (Figure 1)

$$\Delta u + k^2 u = f, \tag{1.1}$$

*Courant Institute, New York University, New York, NY. Email: lai@cims.nyu.edu

†Courant Institute, New York University, New York, NY and Simons Foundation, New York, NY. Email: greengard@cims.nyu.edu

‡Courant Institute and School of Engineering, New York University, New York, NY. Email: oneil@cims.nyu.edu

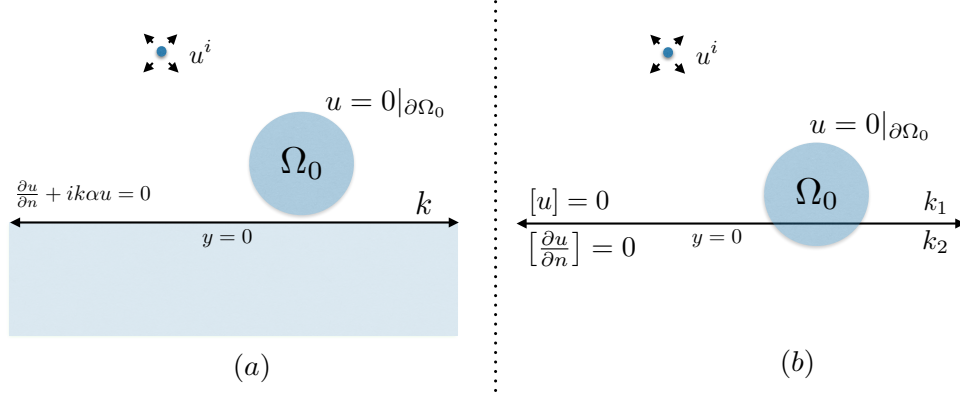


Figure 1: (a) Scattering in the presence of an impedance half-space, with a point source defining the incoming field and a sound soft scatterer Ω_0 . In (b), the impedance boundary is replaced by two-layer media, with a distinct Helmholtz parameter in the lower half-space. The scatterer Ω_0 is partially buried and touches both media.

with boundary conditions enforced on a scatterer Ω_0 and interface conditions enforced on the line $y = 0$, either of impedance (Robin) type

$$\frac{\partial u}{\partial n} + ik\alpha u = 0, \quad (1.2)$$

or of transmission type

$$[u] = 0, \quad \left[\frac{\partial u}{\partial n} \right] = 0. \quad (1.3)$$

The Helmholtz coefficient k is given as $k = \omega/c$, where ω is the governing frequency and c is the wave speed in the medium. For the sake of simplicity, we will assume that on the scatterer Ω_0 the total field u satisfies homogeneous Dirichlet boundary conditions

$$u = 0|_{\partial\Omega_0}.$$

In electromagnetics, this condition corresponds to the case of scattering from a perfectly conducting obstacle in transverse-magnetic (TM) polarization, and in acoustics to the case of a sound-soft obstacle. Here and in what follows, $\mathbf{n} = (0, 1)$ is the unit normal on the line $y = 0$, $\frac{\partial u}{\partial n}$ denotes the partial derivative of u in the normal direction, and α is an impedance constant [9] with $\Re(\alpha) \geq 0$. The expression $[f]$ denotes the jump in the function f across the line $y = 0$, which we will denote by Γ in the remainder of the paper. We will denote by u^i the incoming field induced by the sources f in (1.1). We will limit our attention, without loss of generality, to either point sources or plane waves. To ensure uniqueness of the boundary value problem, a radiation condition must be imposed to enforce that the scattered field is decaying. Thus, we assume that the total field u is written in the form $u = u^i + u^s$, where the scattered field u^s

satisfies the Sommerfeld radiation condition [11]:

$$\lim_{r \rightarrow \infty} \sqrt{r} \left(\frac{\partial u^s}{\partial r} - iku^s \right) = 0. \quad (1.4)$$

We will also assume that the Helmholtz parameter k is constant in either the upper or lower half-space, with $\Re(k) > 0$ and $\Im(k) \geq 0$. Some applications require variants of the interface conditions above, such as

$$[\gamma u] = f, \quad \left[\beta \frac{\partial u}{\partial n} \right] = g, \quad (1.5)$$

where γ, β are piecewise constant material parameters [10, 22–24]. The method of this paper extends to these cases in a straightforward manner.

Integral equations are natural candidates for solving the problems described above since they discretize the scatterer alone and impose the Sommerfeld radiation condition by construction. In order to make effective use of this approach, however, one must generally evaluate the governing Green’s function which satisfies the homogeneous interface conditions (1.2) or (1.3). This avoids the need to discretize the interface Γ (the infinite line $y = 0$), and the most common treatment, using Fourier analysis, was pioneered by Sommerfeld, Weyl and Van der Pol [34, 37, 38]. Over the past several decades, a number of methods have been developed, based on this approach. These include using ideas from high-frequency asymptotics, rational approximation, contour deformation [7, 8, 27, 31, 32], complex images [26, 35, 36], and methods based on special functions [19] or physical images [29].

Without reviewing the methods listed above in detail, we simply note that all of them are aimed at the efficient pointwise evaluation of the impedance or layered media Green’s function, rather than treating the scattering problem itself in a more unified fashion. Here, we consider a substantially different approach, motivated by the fact that close-to-touching interactions between compactly supported scatterers are easily accounted for using standard *physical space* layer potentials, which can be adaptively refined to cope with the near singularities induced by the geometry (see, for example, [13, 16, 17]). Potential theory cannot be used naively in layered media, however, because of the infinite extent of the interface. In principle, however, it seems plausible that the failure of rapid convergence of the Sommerfeld integral is due entirely to the close-to-touching interaction. This turns out to be the case, and we present a rigorous, hybrid method for scattering problems that combines the best features of layer potentials (adaptivity with high order convergence) and of the Sommerfeld representation (spectral accuracy for smooth functions). Put differently, layer potentials in physical space will be used to capture features of the solution with high-frequency components in the Fourier domain, and the Sommerfeld integral will be responsible only for the remaining low-frequency components. For this we solve a local integral equation and apply a smooth window function to the solution in order to capture the most singular behavior.

Remark 1. It is worth emphasizing that window functions have been used previously to accelerate the evaluation of layered media Green's functions [7, 8, 31, 32]. The approach in those papers, however, is based on using carefully chosen partitions of unity and asymptotic analysis to evaluate slowly decaying and oscillatory Sommerfeld integrals for each source and target. We are using a partition of unity in *physical* space to enforce rapid decay in a single Sommerfeld-type correction that can be used for all target points.

Bruno and collaborators [5, 6] have independently developed a method that makes use of the same underlying intuition. They also propose using a window function regularizing the integral operator in physical space in order to handle the most complicated features of the scattering problem. Unlike our scheme, asymptotic methods and stationary phase arguments are used to approximate the solution of the integral equation on the entire interface. Their windowing scheme could be adapted for use in place of our local integral equation (described below), with the potential for eliminating the artificial endpoint singularities introduced in our scheme. This would reduce the complexity of the implementation [4].

An outline of the paper is as follows: in Section 2, we review some basic properties of the free-space Green's function, layer potentials, and their spectral representation. In Sections 3 and 4, we focus on the construction of a *local* integral equation and describe our hybrid representation in more detail. We then prove, in Section 5, that our local integral equation is well-posed. In Section 6, we prove decay estimates on the integrand of our Sommerfeld correction. Section 7 contains some illustrative examples for both pointwise evaluation of the Green's function and for scattering computations in the presence of obstacles. Section 8 contains some brief, concluding remarks.

2 Spectral representation of the Green's function

For $k \in \mathbb{C}$ with non-negative imaginary part, it is well-known that the Green's function for the free-space Helmholtz equation (1.1) is the zeroth order Hankel function of the first kind:

$$G_k(\mathbf{x}, \mathbf{x}_0) = \frac{i}{4} H_0^{(1)}(k|\mathbf{x} - \mathbf{x}_0|). \quad (2.1)$$

It satisfies

$$(\Delta + k^2)G_k(\mathbf{x}, \mathbf{x}_0) = \delta(\mathbf{x} - \mathbf{x}_0), \quad (2.2)$$

where $\delta(\mathbf{x} - \mathbf{x}_0)$ represents the delta function at \mathbf{x}_0 . The Sommerfeld integral representation for $H_0^{(1)}$ is obtained by taking the Fourier transform of equation (2.2) with Fourier coordinates (λ_x, λ_y) , and evaluating the integral in λ_y via contour integration [34, 37, 38]. This yields

$$G_k(\mathbf{x}, \mathbf{x}_0) = \frac{1}{4\pi} \int_{-\infty}^{\infty} \frac{e^{-\sqrt{\lambda^2 - k^2}|y - y_0|}}{\sqrt{\lambda^2 - k^2}} e^{i\lambda(x - x_0)} d\lambda. \quad (2.3)$$

Since λ_x is the only Fourier variable remaining after contour integration, we denote it simply by λ .

The formula (2.3) plays a central role in scattering theory, and numerous schemes are available that yield high order accuracy upon discretization. The simplest, perhaps, is contour deformation to avoid the square root singularity in the integrand (see for example, [2, 10]). We do not review the literature here, since we are primarily concerned with the range of integration required in the Fourier integral parameter λ . The relevant considerations are most easily understood in the context of computing the Green's function for a perfectly conducting or sound-soft half-space, where we seek to impose the Dirichlet condition $u = 0$ on the interface Γ .

The obvious solution, of course, is to construct the corresponding Green's function, which we denote by G_k^0 , using the method of images. Assuming $\mathbf{x}_0 = (x_0, y_0)$ with $y_0 > 0$, let its reflected image $\mathbf{x}_0^R = (x_0, -y_0)$. It is then easy to verify that

$$G_k^0(\mathbf{x}, \mathbf{x}_0) = \frac{i}{4} H_0^{(1)}(k|\mathbf{x} - \mathbf{x}_0|) - \frac{i}{4} H_0^{(1)}(k|\mathbf{x} - \mathbf{x}_0^R|). \quad (2.4)$$

Using the Sommerfeld integral, we may instead write

$$G_k^0(\mathbf{x}, \mathbf{x}_0) = \frac{i}{4} H_0^{(1)}(k|\mathbf{x} - \mathbf{x}_0|) - \frac{1}{4\pi} \int_{-\infty}^{\infty} \frac{e^{-\sqrt{\lambda^2 - k^2}|y + y_0|}}{\sqrt{\lambda^2 - k^2}} e^{i\lambda(x - x_0)} d\lambda. \quad (2.5)$$

While this is more complicated than (2.4), the analogous approach can be used even when the boundary or interface condition does not support a simple image representation, as we shall see below. For the moment, we simply wish to observe that when $|y + y_0|$ is large, the integrand in (2.5) is rapidly decaying, once $\Re(\lambda^2 - k^2) > 0$. When $|y + y_0|$ is small, however, the decay is negligible and the range required in λ is large. In this regime, the Sommerfeld representation is extremely inefficient unless various asymptotic or contour deformation methods are employed.

A third approach to imposing the homogeneous Dirichlet interface condition $u = 0$ on Γ is to write $u(\mathbf{x}) = \frac{i}{4} H_0^{(1)}(k|\mathbf{x} - \mathbf{x}_0|) + u^s(\mathbf{x})$, with the scattered field u^s represented as a double layer potential with unknown density σ :

$$u^s(\mathbf{x}) = D_\Gamma^k[\sigma](\mathbf{x}) \equiv \int_\Gamma \left[\frac{\partial}{\partial n'} G_k(\mathbf{x}, \mathbf{x}') \right] \sigma(\mathbf{x}') ds(\mathbf{x}'). \quad (2.6)$$

Here s denotes arclength along Γ , and $\partial/\partial n'$ denotes differentiation in the outward normal direction at the point \mathbf{x}' . Substituting the representation of u^s into the boundary condition $u = 0$ yields a second-kind integral equation:

$$\frac{\sigma}{2} + D_\Gamma^{k*}[\sigma] = -u^i, \quad (2.7)$$

where D_Γ^{k*} denotes the principal value of D_Γ^k . On a half-space, however, it is well-known that

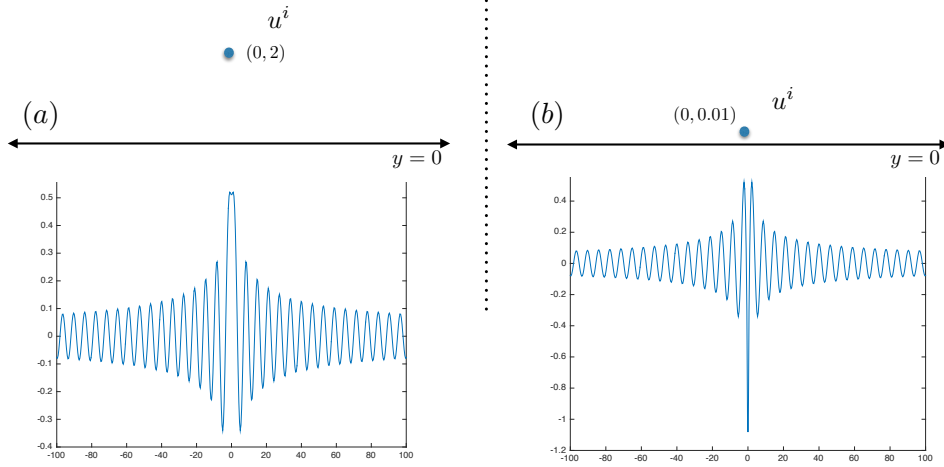


Figure 2: (a) For a point source at $(0, 2)$ with $k = 1$, we plot the imaginary part of the function u^i on Γ . The response is smooth, oscillates over the indicated range $(-100, 100)$, and decays slowly (like $1/\sqrt{x}$). (b) When the point source is near Γ , the oscillations and slow decay are still present, but the function is nearly singular at the close-to-touching point.

D_{Γ}^{k*} vanishes [15], so that $\sigma = -2u^i$ and

$$u^s(x) = D_{\Gamma}^k [-2u^i](x).$$

This is not useful in practice, because $\Gamma = (-\infty, \infty)$ and u^i is slowly decaying in space, so that the range of integration is extremely large (see Figure 2). Note, however, that when y_0 is small, u^i is nearly singular only at the close to touching point in physical space. This accounts for the slow convergence of the integrand in the Sommerfeld integral, $\frac{e^{-\sqrt{\lambda^2 - k^2}y_0}}{\sqrt{\lambda^2 - k^2}} e^{-i\lambda x_0}$, which is simply the Fourier transform of u^i along the line Γ .

Our hybrid approach is based on the following premise: that the poor convergence of the Sommerfeld integral is due entirely to the near singularity in the layer potential density ($\sigma = -2u^i$) at the close-to-touching point. Thus, we partition u^i into a local part, for which we may make effective use of layer potentials, and a remainder, for which we can effectively use the Sommerfeld representation (see Figure 3).

More precisely, let us assume we have a window function $W(x) \in C^{\infty}(\mathbb{R})$, supported on a finite section of the interface, $\Gamma_0 = (-M_0, M_0)$, that satisfies

$$W(x) = \begin{cases} 0 & \text{for } x \leq -3/4M_0, \\ 1 & \text{for } -1/4M_0 \leq x \leq 1/4M_0, \\ 0 & \text{for } x \geq 3/4M_0. \end{cases} \quad (2.8)$$

We can construct such a window function from a compactly supported C^{∞} function, such as

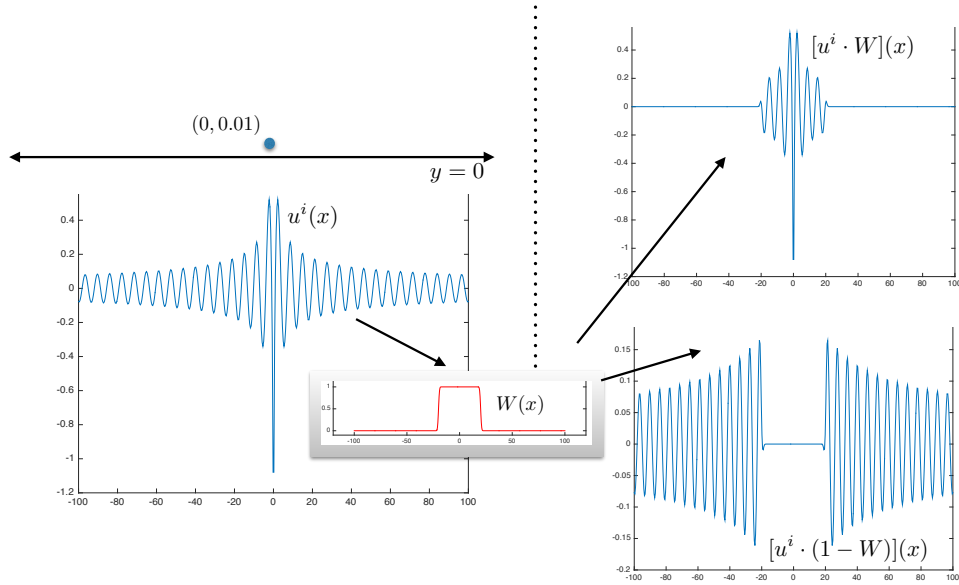


Figure 3: For a point source near the boundary, the double layer density $2u^i$ is nearly singular on Γ . We use a smooth window function (see text) to capture the nearly singular part in physical space (top right), and the Sommerfeld integral to account for the remainder (bottom right).

the standard *bump* function:

$$\Psi(x) = \begin{cases} e^{-\frac{1}{1-x^2}} & \text{for } |x| < 1; \\ 0 & \text{otherwise.} \end{cases}$$

For this, we let $\Phi(x) = \frac{1}{A} \int_0^x \Psi(t) dt$, where $A = \int_0^1 \Psi(t) dt$, and define

$$W(x) = W_{M_0}(x) = \frac{1}{2} (\Phi(x + M_0/2) - \Phi(x - M_0/2)). \quad (2.9)$$

It is straightforward to verify that, once $M_0 > 4$, $W(x)$ satisfies the desired conditions. We use notations W and W_{M_0} interchangeably, depending on the particular relevance of the parameter M_0 .

Remark 2. In practice, we use

$$\tilde{W}(x) = \tilde{W}_{M_0}(x) = 1/2 (\operatorname{erf}(x + M_0/2) - \operatorname{erf}(x - M_0/2)) \quad (2.10)$$

where $\operatorname{erf}(x)$ is the error function

$$\operatorname{erf}(x) = \frac{2}{\sqrt{\pi}} \int_0^x e^{-t^2} dt. \quad (2.11)$$

When $M_0 = 28$, \tilde{W} in (2.10) satisfies (2.8) with more than fourteen digits of accuracy. For

smaller windows (smaller values of M_0), \tilde{W} can simply be rescaled. The smaller the window, however, the less rapid the decay of its Fourier transform.

Letting $\sigma_W(x) = W(x) \cdot \sigma(x) = W_{M_0}(x) \cdot (-2u^i(x))$, we seek to represent the scattered field in the form

$$u^s(x) = \int_{\Gamma_0} \left[\frac{\partial}{\partial n'} G_k(x, x') \right] \sigma_W(x') ds(x') + \frac{1}{4\pi} \int_{-\infty}^{\infty} e^{-\sqrt{\lambda^2 - k^2}y} e^{i\lambda x} \hat{\xi}_W(\lambda) d\lambda. \quad (2.12)$$

Using the decomposition $\sigma = \sigma_W + (1 - W)\sigma$, it is straightforward to verify that

$$\hat{\xi}_W(\lambda) = -2 \widehat{(1 - W)} * \left(\frac{e^{-\sqrt{\lambda^2 - k^2}y_0}}{\sqrt{\lambda^2 - k^2}} e^{-i\lambda x_0} \right), \quad (2.13)$$

where $\hat{f}(\lambda)$ denotes the Fourier transform of $f(x)$:

$$\hat{f}(\lambda) = \int_{-\infty}^{\infty} f(x) e^{-i\lambda x} dx.$$

That is, u^s is represented as a double layer potential over a finite region Γ_0 plus a Sommerfeld correction with density $\hat{\xi}_W$, defined in (2.13). It turns out that $\hat{\xi}_W$ is rapidly decaying as a function of λ , as shown in Theorem 2.2 below. In subsequent sections, we show how this hybrid representation can be applied to the cases of interest, rather than merely the Dirichlet problem where one would (of course) use the simple image solution in practice.

Lemma 2.1. *The Fourier transform of the window function W_{M_0} in (2.10) decays superalgebraically.*

Proof. This follows immediately from the fact that W is C^∞ and integration by parts. \square

Theorem 2.2. *Let u^s be the scattered field induced by a point source at $(0, h)$ satisfying the Dirichlet boundary condition $u^s = -u^i$. If we represent u^s in the form (2.12), then $|\hat{\xi}_W(\lambda)|$ decays superalgebraically, independent of h .*

Proof. Rather than deriving this estimate directly from formula (2.13), we write

$$\hat{\xi}_W(\lambda) = -2 \left[\widehat{1 - W_{M_0}} * \widehat{u^i} \right] = -2 \left[\widehat{1 - W_{M_0}} * (\widehat{u^i} - \widehat{u_{M_0}^i} + \widehat{u_{M_0}^i}) \right],$$

where $u_{M_0}^i$ denotes the field due to a smooth compactly-supported distribution centered at the source point $(0, h)$ of the form

$$\frac{1}{B} W(3|\mathbf{x} - (0, h)|).$$

This scaled version of W vanishes at a distance $M_0/4$ from the center. If we let

$$B = 2\pi \int_0^{M_0/4} J_0(k\rho) W(3|\mathbf{x} - (0, h)|) \rho d\rho,$$

then u^i and u_M^i are identical, once $|x - (0, h)| > M_0/4$. This is easily established by observing that for $|x| > M_0/4$, the multipole expansion induced by the smooth, compactly supported source and the point source are identical. The choice of B follows directly from the Graf addition theorem [28]. Since $1 - W_{M_0}$ is identically zero in the interval $[-M_0/4, M_0/4]$, it is clear that the product $(1 - W_{M_0})(u^i - u_{M_0}^i)$ is identically zero on the real axis. The result now follows from Lemma 2.1 and the fact that $\widehat{u_{M_0}^i}(\lambda)$ decays superalgebraically, independent of h . \square

Definition 2.3. Let the functions $f, g : \mathbb{R} \rightarrow \mathbb{C}$. The functions f and g are said to be *spectrally equivalent* in the far-field if $\overline{(f - g)(1 - W)} = 0$.

Thus, Theorem 2.2 relies on the fact that u^i and $u_{M_0}^i$ are spectrally equivalent in the far field.

3 The impedance Green's function

We now apply the preceding analysis to the case of the impedance Green's function. The impedance Green's function is the solution to the following boundary value problem:

$$\begin{aligned} \Delta G_k^I(\mathbf{x}, \mathbf{x}_0) + k^2 G_k^I(\mathbf{x}, \mathbf{x}_0) &= \delta(\mathbf{x} - \mathbf{x}_0), & y > 0, \\ \frac{\partial G_k^I}{\partial n} + ik\alpha G_k^I &= 0, & y = 0, \end{aligned} \quad (3.1)$$

where $\mathbf{x} = (x, y)$ and $\mathbf{x}_0 = (x_0, y_0)$, with both points located in the upper half-plane. The system (3.1) can be re-written as a scattering problem if we express G^I in two parts:

$$G_k^I(\mathbf{x}, \mathbf{x}_0) = G_k(\mathbf{x}, \mathbf{x}_0) + u^s(\mathbf{x}), \quad (3.2)$$

i.e. the sum of a free-space Helmholtz point-source G_k located at \mathbf{x}_0 and a scattered field (see Figure 1). Because of translation invariance in x , we assume that the point source is located at $\mathbf{x}_0 = (0, h)$ with h small and positive.

Let us now denote by Ω the upper half space $y > 0$ and by $\Gamma = \partial\Omega$ the line $y = 0$. From (1.1) and (1.2), the scattered field $u^s \in C^2(\Omega) \cup C(\overline{\Omega})$ must satisfy

$$\begin{aligned} \Delta u^s + k^2 u^s &= 0 & \text{in } \Omega, \\ \frac{\partial u^s}{\partial n} + ik\alpha u^s &= g & \text{on } \Gamma, \end{aligned} \quad (3.3)$$

where $\mathbf{x} = (x, 0)$ on Γ and

$$g = -\frac{\partial G_k}{\partial n} - ik\alpha G_k. \quad (3.4)$$

The scattered field u^s must also satisfy the radiation condition

$$\lim_{r \rightarrow \infty} \sqrt{r} \left(\frac{\partial u^s}{\partial r} - ik u^s \right) = 0. \quad (3.5)$$

The standard approach for evaluating u^s is to write

$$u^s(\mathbf{x}) = \frac{1}{4\pi} \int_{-\infty}^{\infty} \frac{e^{-\sqrt{\lambda^2 - k^2}y}}{\sqrt{\lambda^2 - k^2}} e^{i\lambda x} \widehat{\xi}(\lambda) d\lambda,$$

where $\widehat{\xi}(\lambda)$ is an unknown function. This represents a solution to the Helmholtz equation, enforces the desired radiation condition, and permits the imposition of the boundary condition in (3.3) mode by mode. It is straightforward to check that

$$\widehat{\xi}(\lambda) = -e^{-\sqrt{\lambda^2 - k^2}h} \frac{\sqrt{\lambda^2 - k^2} + ika}{\sqrt{\lambda^2 - k^2} - ika}.$$

This is a convenient solution when h is large. When h is small, however, the interval of integration must clearly be of the order $1/h$, which can be prohibitive.

While the standard approach to accelerating convergence of the Sommerfeld integral is based on contour integration or some variant of the method of images (including *complex images*), we seek instead to compute u^s using a combination of the Sommerfeld integral and a single layer potential, as we did for the Dirichlet problem above. For this, we let

$$u^s = S_{\Gamma_0}[\sigma_W] + F_{I_0}[\widehat{\xi}_W], \quad (3.6)$$

where

$$S_{\Gamma_0}[\sigma](\mathbf{x}) = \int_{-M_0}^{M_0} G_k(\mathbf{x}, \mathbf{x}') \sigma(\mathbf{x}') ds(\mathbf{x}'), \quad (3.7)$$

$$F_{I_0}[\widehat{\xi}](\mathbf{x}) = \int_{-N_0}^{N_0} \frac{e^{-\sqrt{\lambda^2 - k^2}y}}{\sqrt{\lambda^2 - k^2}} e^{i\lambda x} \widehat{\xi}(\lambda) d\lambda. \quad (3.8)$$

Here, Γ_0 is the finite segment $(-M_0, M_0)$ on the physical interface Γ and $I_0 = (-N_0, N_0)$ is a finite segment in the Fourier transform domain. We assume $\sigma_W \in C(\Gamma_0)$ and $\widehat{\xi}_W \in C(I_0)$. Note that $\sigma(\mathbf{x}') = \sigma(x')$ with $\mathbf{x}' = (x', 0)$ on Γ_0 .

Unlike the Dirichlet problem, we do not have an analytic formula for the single layer density σ and cannot determine σ_W by a simple windowing procedure. Instead, we first determine a density σ on Γ_0 by letting

$$u_1^s = S_{\Gamma_0}[\sigma]$$

and enforcing the boundary conditions in (3.3) only on the interval $[-M_0, M_0]$. Using standard jump conditions [11, 15], this leads to the *local* integral equation

$$-\frac{1}{2}\sigma + ika S_{\Gamma_0}[\sigma] = g \quad (3.9)$$

on Γ_0 . We will show that $\sigma \in C(\Gamma_0)$ for smooth right-hand-side functions g . After finding σ ,

we define σ_W by

$$\sigma_W = W_{M_0} \sigma, \quad (3.10)$$

as above.

Given σ_W from (3.10), we may substitute it into (3.6) and solve for $\widehat{\xi}_W$ in the Fourier domain:

$$\widehat{\xi}_W(\lambda) \left(-1 + \frac{i k \alpha}{\sqrt{\lambda^2 - k^2}} \right) = e^{-\sqrt{\lambda^2 - k^2} h} \left(1 + \frac{i k \alpha}{\sqrt{\lambda^2 - k^2}} \right) + \frac{1}{2} \widehat{\sigma}_W - i k \alpha \widehat{S_{\Gamma_0} \sigma_W} \quad (3.11)$$

for each $\lambda \in I_0$. We discuss the well-posedness of the local integral equation in Section 5 and show in Section 6 that $\widehat{\xi}_W$ decays exponentially, in a manner controlled by M_0 , the length of the window interval Γ_0 , independent of the source location h .

4 The layered media Green's function

The scheme described above for impedance boundary conditions can be extended in a straightforward manner to the case of layered media. For simplicity, we assume there is a single material interface, Γ , that the wavenumber is k_1 in the upper layer $\Omega_1 = \{y > 0\}$, and that the wavenumber is k_2 in the lower layer $\Omega_2 = \{y < 0\}$. The layered media Green's function is the solution to the boundary value problem:

$$\begin{aligned} \Delta G_{lm}(\mathbf{x}, \mathbf{x}_0) + k_1^2 G_{lm}(\mathbf{x}, \mathbf{x}_0) &= \delta(\mathbf{x} - \mathbf{x}_0), & y > 0, \\ \Delta G_{lm}(\mathbf{x}, \mathbf{x}_0) + k_2^2 G_{lm}(\mathbf{x}, \mathbf{x}_0) &= 0, & y < 0, \end{aligned} \quad (4.1)$$

subject to continuity conditions on Γ of the form

$$[u] = 0, \quad \left[\frac{\partial u}{\partial n} \right] = 0. \quad (4.2)$$

We assume that the source lies in the upper half-space at $\mathbf{x}_0 = (0, h)$, radiating at wavenumber k_1 . We then represent the total field in the top and bottom layers as

$$\begin{aligned} u_1(\mathbf{x}) &= u_1^s(\mathbf{x}) + G_{k_1}(\mathbf{x}, \mathbf{x}_0), & \text{for } \mathbf{x} \in \Omega_1, \\ u_2(\mathbf{x}) &= u_2^s(\mathbf{x}), & \text{for } \mathbf{x} \in \Omega_2. \end{aligned} \quad (4.3)$$

By analogy with the impedance case, we represent the scattered field in the form

$$\begin{aligned} u_1^s &= S_{\Gamma_0}^{k_1}[\sigma_W] + D_{\Gamma_0}^{k_1}[\mu_W] + F_{I_0}^{k_1}[\widehat{\xi}_{W,1}], & \text{for } \mathbf{x} \in \Omega_1, \\ u_2^s &= S_{\Gamma_0}^{k_2}[\sigma_W] + D_{\Gamma_0}^{k_2}[\mu_W] + F_{I_0}^{k_2}[\widehat{\xi}_{W,2}], & \text{for } \mathbf{x} \in \Omega_2, \end{aligned} \quad (4.4)$$

where σ and μ are unknown charge and dipole densities on Γ_0 . Note that the Sommerfeld densities $\widehat{\xi}_{W,1}$ and $\widehat{\xi}_{W,2}$ are distinct, one invoked for the upper layer and one for the lower

layer. As above, we first solve a *local* integral equation on Γ_0 to obtain functions σ and μ . The integral equation is derived by enforcing the continuity conditions (4.2), and classical potential theory yields

$$\begin{aligned}\mu + (S_{\Gamma_0}^{k_1} - S_{\Gamma_0}^{k_2})[\sigma] &= -G_{k_1}(\cdot, \mathbf{x}_0), \\ -\sigma + (T_{\Gamma_0}^{k_1} - T_{\Gamma_0}^{k_2})[\mu] &= -\frac{\partial G_{k_1}(\cdot, \mathbf{x}_0)}{\partial n},\end{aligned}\tag{4.5}$$

where $T_{\Gamma_0}^k$ is the normal derivative of the double layer potential $D_{\Gamma_0}^k$ on Γ_0 , respectively [11, 15]. Once equation (4.5) is solved, we let

$$\begin{aligned}\sigma_W &= W_{M_0} \sigma, \\ \mu_W &= W_{M_0} \mu.\end{aligned}\tag{4.6}$$

We then substitute σ_W and μ_W into the representation (4.4). Taking the Fourier transform, we enforce the continuity conditions (4.2) frequency by frequency, and obtain $\hat{\xi}_{W,1}$ and $\hat{\xi}_{W,2}$.

5 Well-posedness of the integral equation

Our method relies on the solvability of equations (3.9) and (4.5).

Theorem 5.1. *Let g be a Hölder continuous function on Γ_0 with exponent $\alpha > 0$, that is, $g \in C^{0,\alpha}(\Gamma_0)$. Then there exists a unique solution $\sigma \in C(\Gamma_0)$ to the integral equation*

$$-\frac{1}{2}\sigma + ik\alpha S_{\Gamma_0}[\sigma] = g.\tag{5.1}$$

Proof. Since S_{Γ_0} is a compact operator from $C(\Gamma_0)$ to $C(\Gamma_0)$ [11], we may obtain the desired result by means of the Fredholm alternative and simply show uniqueness for the homogeneous case. Thus, assume $g = 0$ and let

$$v(\mathbf{x}) = S_{\Gamma_0}[\sigma](\mathbf{x}) \quad \text{for } \mathbf{x} \in \mathbb{R}^2 \setminus \Gamma_0.\tag{5.2}$$

A simple calculation shows that v satisfies the boundary value problem

$$\begin{aligned}\Delta v + k^2 v &= 0 && \text{in } \mathbb{R}^2 \setminus \Gamma_0, \\ \frac{\partial v^+}{\partial n} + ik\alpha v^+ &= 0 && \text{on } \Gamma_0, \\ \frac{\partial v^-}{\partial n} - ik\alpha v^- &= 0 && \text{on } \Gamma_0,\end{aligned}\tag{5.3}$$

where

$$\begin{aligned} v^\pm(\mathbf{x}) &= \lim_{\delta \rightarrow 0^+} v(\mathbf{x} \pm \delta n(\mathbf{x})), \\ \frac{\partial v^\pm(\mathbf{x})}{\partial n} &= \lim_{\delta \rightarrow 0^+} n(\mathbf{x}) \cdot \nabla v(\mathbf{x} \pm \delta n(\mathbf{x})), \end{aligned} \quad (5.4)$$

for $\mathbf{x} \in \Gamma_0$. The system (5.3) defines an impedance problem on the open arc Γ_0 , which has a unique solution [20]. With zero boundary data, it has only the trivial solution, so that

$$\sigma = \frac{\partial v^-}{\partial n} - \frac{\partial v^+}{\partial n} = 0. \quad (5.5)$$

□

Remark 3. It is important to note that in the preceding theorem, Γ_0 is an open interval. The density σ generally exhibits singularities at the end points [20, 30].

Remark 4. When $h > 0$, $g \in C^\infty(\Gamma_0)$ in equation (3.9) and S_{Γ_0} is a pseudo-differential operator of order minus-one [25]. This implies that $\sigma = 2(ik\alpha S_{\Gamma_0}\sigma - g) \in C^{0,\alpha}(\Gamma_0)$ with $0 < \alpha < 1$. Thus, $\sigma \in C^\infty(\Gamma_0)$.

Remark 5. The proof of existence and uniqueness for the local integral equation in the layered media case is analogous and omitted.

6 Exponential decay of the Sommerfeld integral

In this section, we outline a proof of the fact that $\hat{\xi}_W$ in (3.11) is rapidly decaying, independent of the source location h . The dielectric case is more involved but the proof follows from the same reasoning.

Theorem 6.1. *Let u^s be the scattered field induced by a point source at $(0, h)$ satisfying (3.3). If we represent u^s in the form (3.6), then $|\hat{\xi}_W(\lambda)|$ decays superalgebraically, independent of h .*

Sketch of proof. Rewriting (3.11) slightly, $\hat{\xi}_W$ satisfies

$$\begin{aligned} \left(-1 + \frac{ik\alpha}{\sqrt{\lambda^2 - k^2}}\right) \hat{\xi}_W &= \hat{g} + \frac{1}{2}\widehat{\sigma}_W - ik\alpha \widehat{S_{\Gamma_0}[\sigma_W]} \\ &= \hat{g} - \widehat{g}_W + \left(\widehat{g}_W + \frac{1}{2}\widehat{\sigma}_W - ik\alpha \widehat{S_{\Gamma_0}[\sigma_W]}\right) \\ &= \hat{g} - \widehat{g}_W + \widehat{W \cdot \left(g + \frac{1}{2}\sigma - ik\alpha S_{\Gamma_0}[\sigma]\right)} + ik\alpha \widehat{W \cdot S_{\Gamma_0}[(1-W)\sigma]} \\ &\quad - ik\alpha \widehat{(1-W)S_{\Gamma_0}[\sigma_W]}. \end{aligned} \quad (6.1)$$

Each of these terms satisfies the desired superalgebraic decay estimate. The result for $\hat{g} - \widehat{g}_W$ follows the proof of Theorem 2.2. The second term vanishes since it is the Fourier transform of the residual from solving the local integral equation. (In practice, it is zero to discretization error.) The third term is complicated since the solution of the local integral equation, σ , is singular

at the endpoints of Γ_0 . However, the frequency content of $S_{\Gamma_0}[(1 - W)\sigma]$ is controlled near the origin, and multiplication by $W = W_{M_0}$ restricts the function to the interval $[-3M_0/4, 3M_0/4]$. The last term follows from the spectral equivalence in the far field of $S_{\Gamma_0}[\sigma_W]$ and a mollified version of σ_W . \square

We state without proof the analogous result for the dielectric case.

Theorem 6.2. *Let u^1 and u^2 denote the total fields for $y > 0$ and $y < 0$, respectively, satisfying the continuity conditions (4.2), with a point source in the upper medium at $(0, h)$. If we represent u^s in the form (4.4), then $|\hat{\xi}_{W,1}(\lambda)|$ and $|\hat{\xi}_{W,2}(\lambda)|$ decay superalgebraically, independent of h .*

7 Numerical examples

In the experiments described below, all of the local integral equations are solved using Nyström discretization on panels, each containing (scaled) 16th-order Legendre nodes. We use generalized Gaussian quadrature for the self-interaction panels, following the approach described in [3, 16]. Off-panel evaluation is carried out using Quadrature By Expansion (QBX) [1, 12, 18] and the resulting linear systems are solved iteratively using GMRES [33].

We fix the parameters $M_0 = 20$ and $N_0 = 30$ for all examples, and as mentioned before, use the window function in (2.10). To accurately evaluate the Sommerfeld integral and avoid the square root singularity in the integrand, we deform the integration contour along a hyperbolic tangent curve:

$$\lambda(t) = t - \frac{\tanh(t)}{2}i, \quad t \in [-30, 30]. \quad (7.1)$$

This contour is then discretized using 600 uniformly distributed points in t , and the integral is evaluated by mean of the trapezoidal rule (which will converge exponentially fast in this case).

7.1 Impedance Green's function evaluation

Our first example is simply the evaluation of the impedance Green's function for a source located very near to the interface. We set the impedance constant α in equation (1.2) to be $\alpha = 1 - 0.1i$. Numerical results are shown in Table 1 and Figure 4.

Figure 4 plots the result when the source is located at $(0, 10^{-8})$ for wavenumber $k = 10$. One can see a sharp spike in the charge density σ which causes slow convergence in the Fourier domain. However, once we apply the window function to the local integral equation, the resulting Sommerfeld density has a rapidly decaying Fourier transform, as shown in Figure 4c. By the time $\lambda = 30 - \frac{\tanh(30)}{2}i$, $\hat{\xi}_W$ is already less than 10^{-10} . The density σ was discretized along Γ_0 using 160 panels, adaptively refined toward the origin. This required 2560 discretization nodes.

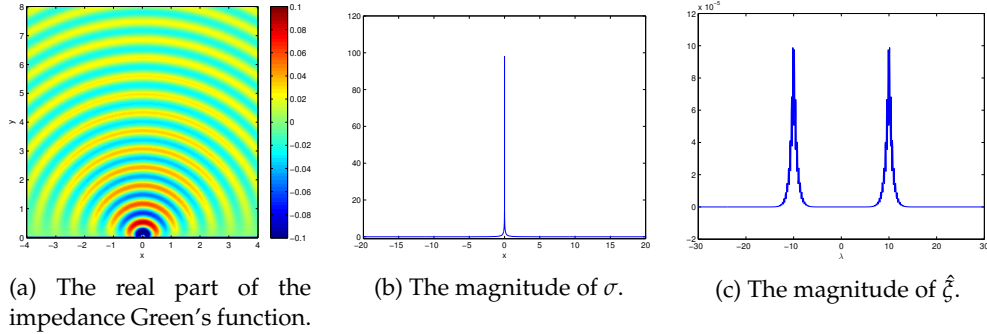


Figure 4: The impedance Green's function, along with magnitudes of the layer potential density σ and the Sommerfeld integral density $\hat{\zeta}_W$.

Wavenumber k	1	1	10	10	$20+i$	$20+i$
Height h	$1e-5$	$1e-8$	$1e-5$	$1e-8$	$1e-5$	$1e-8$
$\hat{\zeta}(-30)$	$7.99e-16$	$2.15e-16$	$2.06e-11$	$2.06e-11$	$4.83e-11$	$4.83e-11$
Error	$3.49e-15$	$3.28e-15$	$2.15e-11$	$2.15e-11$	$1.22e-10$	$1.22e-10$

Table 1: Convergence results for the evaluation of the impedance Green's function when the source point is close to the interface.

Table 1 shows the value of the density $\hat{\zeta}_W$ at $t = -30$ in (7.1) and the error in the impedance condition $\partial u / \partial n + ik\alpha u$ at $(2.5, 0)$ for a variety of wavenumbers k and heights h . Note that the error is independent of the height h and that the density $\hat{\zeta}$ has decayed rapidly.

Remark 6. When the source point is very close to the interface, such as $h = 10^{-8}$, the maximal normal derivative of G_k on Γ is of the order $O(1/h)$, while the potential is of the order $O(\log h)$. To avoid catastrophic cancellation, we place an image source at the reflected point across Γ with the same strength as the original source. This cancels the normal derivative of G_k on Γ . It is added back in the final evaluation. We apply the same technique when evaluating the layered media Green's function in the next example. This is a finite precision issue, and independent of our theory. For a general scattering problem, if the net contribution from a continuous charge density on the interface is $O(1)$, as in Example 3, we do not need to carry out this stabilization.

7.2 Layered media Green's function evaluation

In our second numerical example, we evaluate the layered media Green's function. Figure 5 shows the real part of the Green's function for $k_1 = 10$ in the upper half-space and $k_2 = 20$ in the lower half-space with source point at $(0, 10^{-8})$. As in the impedance example, there is a spike in the dipole density μ at $x = 0$. Using *only* a Sommerfeld integral approach would require a prohibitively large interval of integral to obtain convergence, while our hybrid scheme achieves rapid convergence in the Fourier domain, as can be seen from the plot of $\hat{\zeta}_{W,1}$ in Figure 5c. More detailed data concerning errors in evaluating the Green's functions are provided in Table 2. The error is measured as the discrepancy in the potential at $(2.5, 0)$ by evaluating the limits

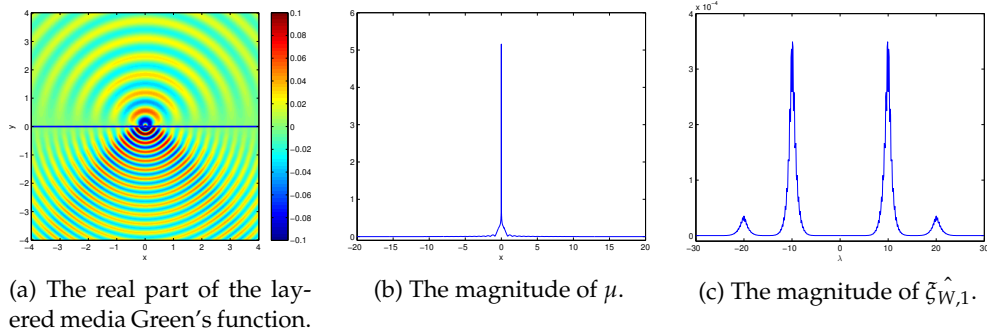


Figure 5: The layered media Green's function, the magnitudes of the layer potential density μ and the Sommerfeld integral density $\hat{\zeta}_{W,1}$.

Wavenumber k_1	1	1	$10+i$	$10+i$	10	10
Wavenumber k_2	5	5	5	5	20	20
Height h	$1e-5$	$1e-8$	$1e-5$	$1e-8$	$1e-5$	$1e-8$
$\hat{\zeta}_1(-30)$	$4.09e-15$	$3.67e-15$	$1.02e-15$	$1.82e-15$	$1.63e-11$	$1.63e-11$
Error	$1.44e-15$	$1.01e-15$	$3.88e-14$	$3.85e-14$	$8.28e-10$	$8.28e-10$

Table 2: Convergence results for the evaluation of the layered media Green's function when the source point is close to the interface.

from above and below. The Sommerfeld density decays rapidly, independent of the height h , consistent with our analysis. As with the impedance problem, 160 panels adaptively refined toward the origin (2560 points) were required for the discretization of σ and μ on Γ_0 .

7.3 Scattering from inclusions

We now show the application of our scheme to solving a scattering problem from an object extremely close to, or partially buried in, a layered media interface. The incident wave is assumed to be generated by a point source located at $(3, 3)$.

7.3.1 Close-to-touching object lying in the upper half-space

We consider a circular object Ω_0 with radius 1 centered at $(0, 1 + \epsilon)$ above the interface. We set $\epsilon = 10^{-10}$, so that the object is only a distance 10^{-10} from the interface Γ . The object is assumed to be a perfect conductor or a sound-soft scatterer, both of which require that we impose zero

Wavenumber k_1	1	1	$10+i$	$10+i$	10	10
Wavenumber k_2	2	5	5	$5+i$	$20+5i$	20
GMRES iter.	9	10	14	14	31	31
$\hat{\xi}_1(-30)$	3.15e-13	1.08e-13	3.54e-14	3.62e-14	1.78e-8	4.06e-8
Error	9.24e-12	1.64e-12	1.32e-10	2.12e-10	1.44e-11	8.04e-11

Table 3: Convergence results for scattering from an object close to the interface of the layered media. The closest distance is 10^{-10} .

Dirichlet conditions on the object. This yields the following boundary value problem:

$$\begin{aligned}
\Delta u + k_1^2 u &= 0, & \text{in } \Omega_1, \\
\Delta u + k_2^2 u &= 0, & \text{in } \Omega_2, \\
u &= 0, & \text{on } \partial\Omega_0, \\
[u] = \left[\frac{\partial u}{\partial y} \right] &= 0, & y = 0,
\end{aligned} \tag{7.2}$$

along with a suitable decay condition at infinity.

To solve this scattering problem, we add an additional unknown dipole density μ_0 on the boundary of the inclusion Ω_0 . The scattered field u^s is then represented by

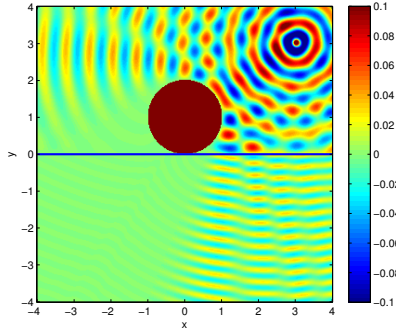
$$u^s = \begin{cases} S_{\Gamma_0}^{k_1}[\sigma_W] + D_{\Gamma_0}^{k_1}[\mu_W] + F_{I_0}^{k_1}[\hat{\xi}_{W,1}] + D_{\partial\Omega_0}^{k_1}[\mu_0] & \text{in } \Omega_1, \\ S_{\Gamma_0}^{k_2}[\sigma_W] + D_{\Gamma_0}^{k_2}[\mu_W] + F_{I_0}^{k_2}[\hat{\xi}_{W,2}] & \text{in } \Omega_2. \end{cases} \tag{7.3}$$

Results for $k_1 = 10$ and $k_2 = 20$ are shown in Figure 6. We only required 120 panels adaptively refined toward the origin (1920 points) for the discretization of σ and μ on Γ_0 . The discretization of μ_0 on $\partial\Omega_0$ required 30 panels.

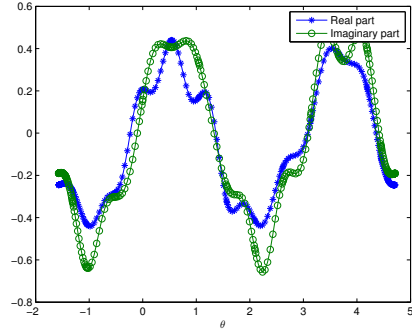
From Figure 6b, the charge density μ_0 on the boundary of the disk behaves rather benignly. However, the density on the interface has a sharp feature near $x = 0$, as expected. Figure 6d shows rapid decay in the Sommerfeld integrand. More detailed errors for various values of the wavenumber in the layered media are shown in Table 3. The GMRES iterations are stopped when the residual is less than 10^{-10} . The errors are obtained by solving an artificial scattering problem with a known exact solution. For this, the field in each domain is defined by a set of free-space sources located in the complement of the domain (see [21] for further details). In all of our tests, the Sommerfeld integrand decays rapidly.

7.3.2 Scattering from a partially buried object

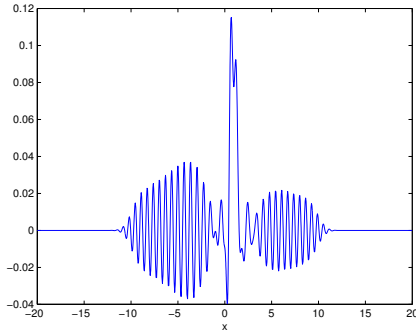
In our final example, a disk of radius 1 crosses the interface between the two layers. The center of the disk is $(0,0)$, and we solve the same boundary value problem as in (7.2). The scattered



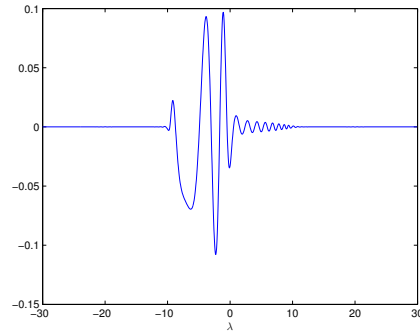
(a) The real part of the total field scattered in the layered media with a circular object located right above the interface.



(b) The real and imaginary parts of the dipole density μ_0 on the boundary of the object



(c) Real part of the charge density σ_W .



(d) Real part of the Sommerfeld density $\hat{\xi}_{W,1}$.

Figure 6: Scattering from an object arbitrarily close to a layered media interface.

field is represented as:

$$u^s = \begin{cases} S_{\Gamma_0}^{k_1}[\sigma_W] + D_{\Gamma_0}^{k_1}[\mu_W] + F_{I_0}^{k_1}[\hat{\xi}_{W,1}] + D_{\partial\Omega_0}^{k_1}[\mu_0] & \text{in } \Omega_1, \\ S_{\Gamma_0}^{k_2}[\sigma_W] + D_{\Gamma_0}^{k_2}[\mu_W] + F_{I_0}^{k_2}[\hat{\xi}_{W,2}] + D_{\partial\Omega_0}^{k_2}[\mu_0] & \text{in } \Omega_2. \end{cases} \quad (7.4)$$

Note that the density μ_0 on the scatterer is used globally – on both sides of the layered media interface. As in the earlier work [14, 21], this has the advantage that the resulting integral equation is of the second kind. Results are shown in Figure 7. The densities $\hat{\xi}_{W,1}$ and $\hat{\xi}_{W,2}$ in the respective Sommerfeld integrals are again rapidly convergent. Along Γ_0 , 180 panels (2880 points) adaptively refined toward the intersection of the inclusion and Γ_0 were used to discretize σ and μ on Γ_0 . Discretizing μ_0 on $\partial\Omega_0$ required 60 panels. Detailed numerical errors are presented in Table 4. The results, again, are consistent with our analysis.

Wavenumber k_1	1	1	$10+i$	$10+i$	10	10
Wavenumber k_2	2	5	5	$5+i$	$20+5i$	20
GMRES iter.	10	13	16	12	16	40
$\hat{\xi}_1(-30)$	7.68e-14	3.78e-14	1.88e-14	1.42e-14	1.41e-9	1.32e-6
Error	3.47e-12	7.41e-12	1.71e-13	4.07e-13	5.18e-10	6.69e-10

Table 4: Convergence results for scattering from a partially buried object in layered media.

8 Conclusions

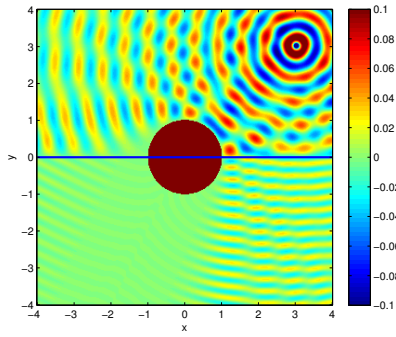
We have constructed a hybrid approach to acoustic wave scattering in layered media or in half-spaces with impedance boundary conditions. Our approach retains the advantages of classical (physical space) layer potentials in handling close-to-touching interactions and the advantages of the Sommerfeld integral in representing smooth interactions along infinite boundaries. By solving a local integral equation and subtracting its effect from the original boundary data, we have shown that the remaining problem can be solved in the Fourier domain with a rapidly convergent integrand.

We have also shown that the hybrid representation is very convenient when solving scattering problems with obstacles (including partial buried obstacles). High-order accurate results are easily obtained without the direct construction of the Green’s function. Instead, our representation splits the problem into a free-space scattering problem posed on obstacles and finite segments, plus a Sommerfeld correction to enforce the boundary condition along the infinite interface. We are currently extending our method to axisymmetric and fully three-dimensional problems in both acoustics and electromagnetics.

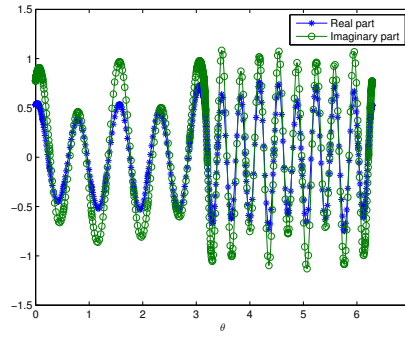
Acknowledgements: We would like to thank Alex Barnett, Charlie Epstein, and Tom Hagstrom for several useful discussions.

References

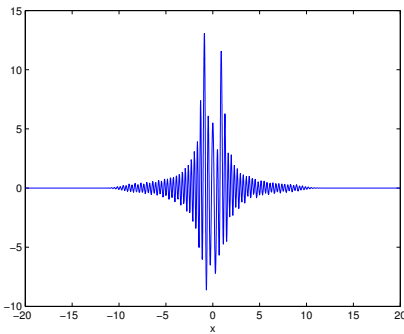
- [1] A. Barnett. Evaluation of layer potentials close to the boundary for Laplace and Helmholtz problems on analytic planar domains. *SIAM J. Sci. Comput.*, 36:A427–A451, 2014.
- [2] A. Barnett and L. Greengard. A new integral representation for quasi-periodic scattering problems in two dimensions. *BIT Numer. Math.*, 51(1):67–90, 2011.
- [3] J. Bremer, Z. Gimbutas, and V. Rokhlin. A nonlinear optimization procedure for generalized Gaussian quadratures. *SIAM J. Sci. Comput.*, 32(4):1761–1788, 2010.
- [4] O. P. Bruno. personal communication. *January*, 2015.



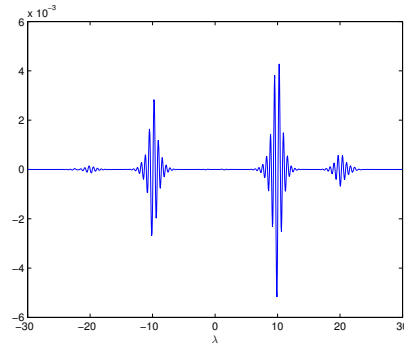
(a) The real part of the total field scattered in the layered media with a circular object partially buried in the layers.



(b) The real and imaginary part of the dipole density μ_0 on the boundary of the object



(c) Real part of the charge density σ .



(d) Real part of the Sommerfeld density $\hat{\zeta}_1$.

Figure 7: Scattering from an object partially buried across a layered media interface.

- [5] O. P. Bruno. Resonances, absorption, waveguides, windowing and scattering poles. *Annual AFOSR Electromagnetic Contractor's Review, Arlington, VA, January, 2015.*
- [6] O. P. Bruno, M. Lyon, C. Pérez-Arancibia, and C. Turc. Windowed Green Function method for layered-media scattering. *arXiv:1507.04445, 2015.*
- [7] W. Cai. *Computational Methods for Electromagnetic Phenomena.* Cambridge University Press, New York, NY, 2013.
- [8] W. Cai and T. J. Yu. Fast Calculations of Dyadic Green's Functions for Electromagnetic Scattering in a Multilayered Medium. *J. Comput. Phys.*, 165(1):1–21, 2000.
- [9] S. N. Chandler-Wilde. The impedance boundary value problem for the Helmholtz equation in a half-plane. *Math. Methods Appl. Sci.*, 20(10):813–840, 1997.
- [10] W. C. Chew. *Waves and Fields in Inhomogeneous Media.* IEEE Press, Piscataway, NJ, 1990.
- [11] D. Colton and R. Kress. *Integral Equation Methods in Scattering Theory.* Wiley-Interscience, New York, 1983.

- [12] C. L. Epstein, A. Klöckner, and L. Greengard. On the Convergence of Local Expansions of Layer Potentials. *SIAM J. Num. Anal.*, 51:2660–2679, 2013.
- [13] L. Greengard and J. Helsing. On the numerical evaluation of elastostatic fields in locally isotropic two-dimensional composites. *J. Mech. Phys. Solids*, 46:1441–1462, 1998.
- [14] L. Greengard, K. Ho, and J.-Y. Lee. A fast direct solver for scattering from periodic structures with multiple material interfaces in two dimensions. *J. Comput. Phys.*, 258:738–751, 2014.
- [15] R. B. Guenther and J. W. Lee. *Partial Differential Equations of Mathematical Physics and Integral Equations*. Dover, 1996.
- [16] S. Hao, A. H. Barnett, P. G. Martinsson, and P. Young. High-order accurate methods for Nyström discretization of integral equations on smooth curves in the plane. *Adv. Comput. Math.*, 40:245–272, 2014.
- [17] J. Helsing. Thin bridges in isotropic electrostatics. *J. Comput. Phys.*, 127:142–151, 1996.
- [18] A. Klöckner, A. Barnett, L. Greengard, and M. O’Neil. Quadrature by Expansion: A new method for the evaluation of layer potentials. *J. Comput. Phys.*, 252:332–349, 2013.
- [19] I.-S. Koh and J.-G. Yook. Exact Closed-Form Expression of a Sommerfeld Integral for the Impedance Plane Problem. *IEEE Trans. Antennas Propag.*, 54(9):2568–2576, 2006.
- [20] R. Kress and K. M. Lee. Integral equation methods for scattering from an impedance crack. *Journal of Computational and Applied Mathematics*, 161(1):161–177, 2003.
- [21] J. Lai, S. Ambikasaran, and L. F. Greengard. A fast direct solver for high frequency scattering from a large cavity in two dimensions. *SIAM J. Sci. Comput.*, 36(6):B887–B903, 2014.
- [22] I. V. Lindell and E. Alanen. Exact Image Theory for the Sommerfeld Half-Space Problem, Part I: Vertical Magnetic Dipole. *IEEE Trans. Antennas Propag.*, 32(2):126–133, 1984.
- [23] I. V. Lindell and E. Alanen. Exact Image Theory for the Sommerfeld Half-Space Problem, Part II: Vertical Electric Dipole. *IEEE Trans. Antennas Propag.*, 32(8):841–847, 1984.
- [24] I. V. Lindell and E. Alanen. Exact Image Theory for the Sommerfeld Half-Space Problem, Part III: General Formulation. *IEEE Trans. Antennas Propag.*, 32(10):1027–1032, 1984.
- [25] W. McLean. *Strongly elliptic systems and boundary integral equations*. Cambridge University Press, Cambridge, 2000.
- [26] M. Ochmann. The complex equivalent source method for sound propagation over an impedance plane. *J. Acoust. Soc. Amer.*, 116(6):3304–3311, 2004.

- [27] V. I. Okhmatovski and A. C. Cangellaris. Evaluation of layered media Greens functions via rational function fitting. *IEEE Microw. Wireles Comp. Lett.*, 14:22–24, 2004.
- [28] F. W. Olver, D. W. Lozier, R. F. Boisvert, and C. W. Clark. *NIST Handbook of Mathematical Functions*. Cambridge University Press, New York, NY, USA, 1st edition, 2010.
- [29] M. O’Neil, L. Greengard, and A. Pataki. On the efficient representation of the half-space impedance Green’s function for the Helmholtz equation. *Wave Motion*, 51:1–13, 2014.
- [30] A. Osipov and A. Norris. The Malyuzhinets theory for scattering from wedge boundaries: a review. *Wave Motion*, 29(4):313–340, 1999.
- [31] M. Paulus, P. Gay-Balmaz, and O. J. F. Martin. Accurate and efficient computation of the Green’s tensor for stratified media. *Physical Review E*, 62:5797–5807, 2000.
- [32] C. Pérez-Arancibia and O. P. Bruno. High-order integral equation methods for problems of scattering by bumps and cavities on half-planes. *Journal of the Optical Society of America A*, 31(8):1738, 2014.
- [33] Y. Saad and M. H. Schultz. GMRES: A Generalized Minimal Residual Algorithm for Solving Nonsymmetric Linear Systems. *SIAM J. Sci. Stat. Comput.*, 7:856–869, 1986.
- [34] A. Sommerfeld. Über die ausbreitung der wellen in der drahtlosen telegraphie. *Ann. Phys. Leipzig*, 28:665–737, 1909.
- [35] G. Taraldsen. The complex image method. *Wave Motion*, 43(1):91–97, 2005.
- [36] D. J. Thomson and J. T. Weaver. The complex image approximation for induction in a multilayered earth. *J. Geophys. Res.*, 80(1):123–129, 1975.
- [37] B. Van der Pol. Theory of the reflection of the light from a point source by a finitely conducting flat mirror, with an application to radiotelegraphy. *Physica*, 2(1–12):843–853, 1935.
- [38] H. Weyl. Ausbreitung elektromagnetischer wellen über einem ebenen leiter. *Ann. Phys. Leipzig*, 60:481–500, 1919.